

Robust Underwater Obstacle Detection for Collision Avoidance

Varadarajan Ganesan, Mandar Chitre and Edmund Brekke

ARL, Tropical Marine Science Institute and
Department of Electrical and Computer Engineering
National University of Singapore
Singapore 119227.

{varadarajan,mandar,edmund}@arl.nus.edu.sg
<http://www.arl.nus.edu.sg>

Abstract. Underwater obstacle detection and avoidance is essential for safe deployment of autonomous underwater vehicles (AUVs). A forward-looking sonar is typically used to detect and localize potential obstacles. Such sensors tend to have a coarser sensor resolution and a lower signal-to-noise ratio (SNR) than electromagnetic sensors typically used for similar tasks in land-based robotics. Lack of access to GPS causes additional uncertainty in vehicle navigation, making it difficult to detect and localize potential obstacles relative to a world-fixed reference frame. In this paper, we propose an obstacle detection algorithm for AUVs which is based on occupancy grids. The proposed method differs from existing occupancy grid-techniques in two key aspects. First, we use an occupancy grid attached to the body frame of the AUV, and not to the world frame. Second, our technique takes detection probabilities and false alarm rates into account, in order to deal with the high amounts of noise present in the sonar data. The proposed algorithm is tested online during field trials at Pandan Reservoir in Singapore and in the sea at Selat Pauh off the coast of Singapore.

Keywords: Underwater Obstacle Detection, Collision Avoidance and Occupancy Grids

1 Motivation

In recent years, we have seen an increasing interest in autonomous underwater navigation and exploration. Although significant advances have been made in the development of autonomous underwater vehicles (AUVs), the technology for effective obstacle avoidance remains relatively immature. Devices such as multibeam and sector-scanning forward looking sonars (FLS) are available for obstacle detection. Although multibeam FLS are commonly adopted as underwater obstacle avoidance sensors due to their superior performance, they are usually much costlier than sector scanning sonars. Our aim in this paper is to develop an algorithm for reliable obstacle detection that may be used with either type of FLS.

We demonstrate our algorithm experimentally using data from the more challenging of the two, i.e., the sector-scanning sonar.

Accurate localization of obstacles is essential for collision avoidance. Due to lack of availability of GPS signals underwater, AUVs generally rely on on-board proprioceptive sensors such as compass, Doppler velocity log (DVL) and inertial navigation system (INS) for underwater navigation. Dead-reckoning using these sensors suffers from unbounded positioning error growth [1], which in turn leads to inaccurate localization of potential obstacles. This problem is even more acute in low-cost AUVs where the proprioceptive sensors have low accuracy.

The conventional approach to solving this problem is to improve the AUV’s positioning accuracy. This may be achieved by using sensors of higher accuracy, or by deploying external aids such as acoustic beacons. Both solutions will incur additional costs. An interesting alternative is to use simultaneous localization and mapping (SLAM) where the detected obstacles are used as landmarks to improve positioning [2, 3]. SLAM holds great promise to solve the navigation and obstacle avoidance problems together, but issues such as feature representation, data association and consistency are still undergoing active research [4]. In our opinion, SLAM is therefore not yet mature enough for reliable underwater obstacle detection and avoidance.

We propose a method for detection and localization of obstacles which employs an occupancy grid attached to the AUV’s body frame. This entails several novelties. Although occupancy grid formulations are popular in land-based robotics [5, 6, 2, 7], this approach does not appear to be common in the underwater domain. Feature-based solutions appear to be more popular [8–11]. Existing publications on occupancy grids for FLS, such as [12] and [13], present results from a controlled environment and under static conditions. In contrast, we present results from both lake trials and sea trials with the AUV in a dynamic state. We believe that the occupancy grid approach is particularly suitable for underwater robotics, since it often is very difficult to extract reliable features from FLS data, especially when a sector-scanning sonar is used.

Furthermore, we use a *local occupancy grid* in the AUV’s frame of reference, as opposed to more conventional geo-referenced occupancy grid. This is somewhat similar to the concept of robocentric SLAM [14]. The key insight underlying this is that for the purpose of obstacle avoidance, as opposed to more comprehensive mapping, the obstacles only need to be accurately localized *relative* to the AUV. Accurate localization in a geo-referenced frame is not necessary. Adopting the AUV’s body frame for obstacle localization makes the obstacle detection and avoidance performance less sensitive to the AUV’s positioning error growth.

Finally, our formulation incorporates motion uncertainties and sensor parameters such as false alarm rate and detection probability in a Bayesian framework. When the AUV moves, the obstacles “move” in the AUV’s body frame in a predictable way. Our *motion model* updates the occupancy probabilities from the estimated translational and rotational motion. When a sonar measurement becomes available, the occupancy probabilities are updated using a Bayesian *measurement model* that integrates new information from the measurement into the belief represented

by the occupancy grid. The occupancy grid is used to determine the location of nearby obstacles. If these obstacles pose a threat of collision, the AUV's command and control system takes evasive maneuvers.

2 Technical Approach

As briefly outlined above, we use a local occupancy grid to represent our belief of the location of nearby obstacles. To update the occupancy grid as the AUV moves and sonar measurements becomes available, we require a motion model and a measurement model. Finally, we require a detection procedure that operates on the occupancy grid to yield a set of potential obstacles. This set of potential obstacles is sent to the AUV's command and control system for consideration of possible avoidance maneuvers.

2.1 Occupancy grid

The local occupancy grid is rectangular with $m \times n$ occupancy cells, each at a fixed location with respect to the AUV. An illustration of the local occupancy grid is shown in Fig. 1. We use $O_{x,y}$ to denote an occupancy cell with index (x, y) . Each occupancy cell $O_{x,y}$ is associated with the events $\mathbb{O}_{x,y}$ that it is occupied and $\widehat{\mathbb{O}}_{x,y}$ that it is not occupied. Therefore, they would be related as $P(\mathbb{O}_{x,y}) + P(\widehat{\mathbb{O}}_{x,y}) = 1$. The $m \times n$ matrix of occupancy probabilities $[P(\mathbb{O}_{x,y}) \forall x, y]$ fully describes the belief held by the algorithm about obstacles in the vicinity of the AUV.

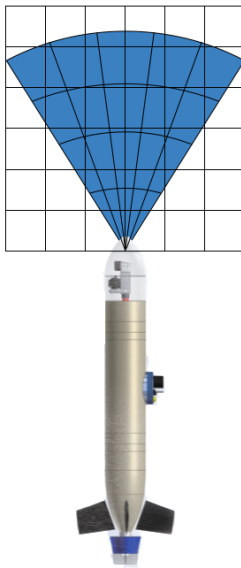


Fig. 1: Illustration of local occupancy grid attached to the AUV and its sensor frame (blue color)

2.2 Measurement model

An FLS sends out a sonar “ping” in a given direction and listens for echoes. The echo intensity profile returned from the environment is discretized into a set of bins (k, θ) where index k represents the range and index θ represents the bearing. Let the measurement observed in bin (k, θ) be $z_{k, \theta}$. Given a threshold value t_k for range bin k , we report a detection $S_{k, \theta} = 1$ if $z_{k, \theta} \geq t_k$ and $S_{k, \theta} = 0$ otherwise.

Let p_k be the probability of detection of an obstacle at a range corresponding to bin k , and f_k be the probability of false alarm which are necessary operational parameters. A plot of p_k vs f_k (parametrized by t_k) is known as the receiver operating characteristic (ROC) curve. This ROC curve varies with signal-to-noise ratio (SNR) and environmental characteristics; we can experimentally measure this for a sonar in an operational environment of interest. We set a constant acceptable false alarm rate f (i.e., set $f_k = f$) and obtain the corresponding p_k and t_k for each range bin k .

The experimentally measured ROC curves matched existing models for detection of targets in the presence of noise as proposed in [15]. At Pandan reservoir, the ROC curves obtained matched that of detection of targets giving constant amplitude returns in Gaussian noise. The model for this case is as follows:

$$p_k = \frac{1}{2} \operatorname{erfc} \left\{ \operatorname{erfc}^{-1}(2f_k) - \sqrt{\frac{\text{SNR}}{2}} \right\} \quad (1)$$

where SNR is the signal to noise ratio, erfc is the complementary error function. This can be explained by the enclosed nature of the reservoir resulting in the presence of Gaussian noise and targets like lake walls with surfaces which would give returns of constant amplitude.

At the sea in Selat Pauh, the background noise did not particularly match any of the existing distribution for background noise models in literature like the Gaussian or Rayleigh distribution. Hence, there is no model for the detection of targets in literature to verify the experimentally obtained ROC curves.

When a measurement becomes available, the occupancy grid serves as a Bayesian prior. Depending on whether $S_{k, \theta} = 1$ ($z_{k, \theta} \geq t_k$) or $S_{k, \theta} = 0$ ($z_{k, \theta} < t_k$), the occupancy cells are updated to the posterior probabilities using Bayes’ rule and the probabilities p_k and f obtained above.

Fig. 2 shows the overlap between occupancy cells and a particular range bin. Let the region of overlap between any range bin (k, θ) and any occupancy cell $O_{x, y}$ be denoted by $O_{k, \theta}^{x, y}$. Also, let $\mathbb{O}_{k, \theta}^{x, y}$ denote the event that the region $O_{k, \theta}^{x, y}$ be occupied. We define our measurement model such that $S_{k, \theta} = 1$ will be observed when a target is present in any one of the overlapping regions $O_{k, \theta}^{x, y}$ with a probability equal to the probability of

detection. This give rise to four possible combination of events as follows:

$$P(S_{k,\theta} = 1 | \mathbb{O}_{k,\theta}^{x,y}) = p_k \quad (2)$$

$$P(S_{k,\theta} = 1 | \widehat{\mathbb{O}}_{k,\theta}^{x,y}) = f \quad (3)$$

$$P(S_{k,\theta} = 0 | \mathbb{O}_{k,\theta}^{x,y}) = 1 - p_k \quad (4)$$

$$P(S_{k,\theta} = 0 | \widehat{\mathbb{O}}_{k,\theta}^{x,y}) = 1 - f \quad (5)$$

Let the area of overlap between range bin (k, θ) and occupancy cell $O_{x,y}$ be $v_{k,\theta}^{x,y}$ and the area of an occupancy cell be denoted by $A(O_{x,y})$. Now the events $\mathbb{O}_{k,\theta}^{x,y}$ and $\mathbb{O}_{x,y}$ are related as follows:

$$P(\mathbb{O}_{k,\theta}^{x,y} | \mathbb{O}_{x,y}) = \frac{v_{k,\theta}^{x,y}}{A(O_{x,y})} = a_{k,\theta}^{x,y} \quad (6)$$

$$P(\widehat{\mathbb{O}}_{k,\theta}^{x,y} | \mathbb{O}_{x,y}) = 1 - a_{k,\theta}^{x,y} \quad (7)$$

$$P(\widehat{\mathbb{O}}_{k,\theta}^{x,y} | \widehat{\mathbb{O}}_{x,y}) = 1 \quad (8)$$

$$P(\mathbb{O}_{k,\theta}^{x,y} | \widehat{\mathbb{O}}_{x,y}) = 0 \quad (9)$$

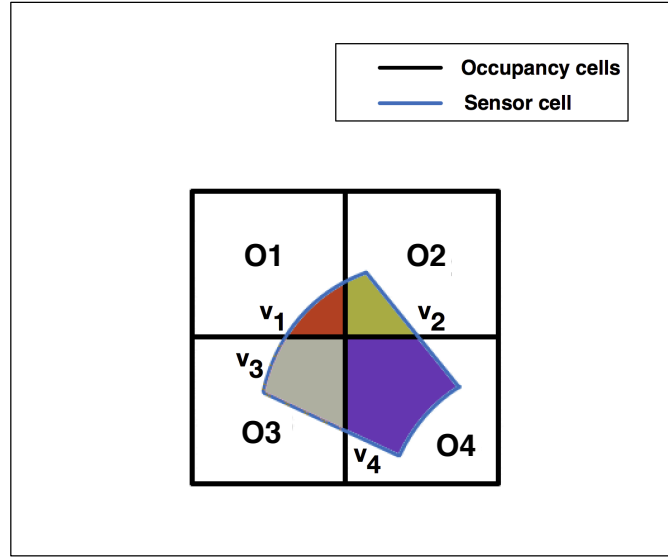


Fig. 2: Illustration of overlap between occupancy cells and a sensor cell. The area of overlap between a range bin and $O\{i\}$, is $v_{\{i\}}$ where $i \in \{1, \dots, 4\}$.

Finally, the map is updated for the two possible cases corresponding to $S_{k,\theta} = 1$ or $S_{k,\theta} = 0$ as follows:

Case 1: Whenever the measurement obtained is such that $S_{k,\theta} = 1$ ($z_{k,\theta} \geq t_k$), the occupancy cell $O_{x,y}$ is updated as follows:

$$P(\mathbb{O}_{x,y} | S_{k,\theta} = 1) = \frac{P(S_{k,\theta} = 1 | \mathbb{O}_{x,y}) P(\mathbb{O}_{x,y})}{P(S_{k,\theta} = 1)} \quad (10)$$

$$P(S_{k,\theta} = 1 | \mathbb{O}_{x,y}) = 1 - P(S_{k,\theta} = 0 | \mathbb{O}_{x,y}) \quad (11)$$

$$\begin{aligned} P(S_{k,\theta} = 0 | \mathbb{O}_{x,y}) &= \prod_{i=1}^m \prod_{j=1}^n \left\{ \sum_{\mathbb{O}_{i,j}} \sum_{\widehat{\mathbb{O}}_{k,\theta}^{i,j}} P(S_{k,\theta} = 0 | \mathbb{O}_{k,\theta}^{i,j}) P(\mathbb{O}_{k,\theta}^{i,j} | \mathbb{O}_{i,j}) P(\mathbb{O}_{i,j} | \mathbb{O}_{x,y}) \right\} \\ &= \prod_{i=1}^m \prod_{j=1}^n \left\{ P(S_{k,\theta} = 0 | \mathbb{O}_{k,\theta}^{i,j}) P(\mathbb{O}_{k,\theta}^{i,j} | \mathbb{O}_{i,j}) P(\mathbb{O}_{i,j} | \mathbb{O}_{x,y}) \right. \\ &\quad + P(S_{k,\theta} = 0 | \widehat{\mathbb{O}}_{k,\theta}^{i,j}) P(\widehat{\mathbb{O}}_{k,\theta}^{i,j} | \mathbb{O}_{i,j}) P(\mathbb{O}_{i,j} | \mathbb{O}_{x,y}) \\ &\quad + P(S_{k,\theta} = 0 | \widehat{\mathbb{O}}_{k,\theta}^{i,j}) P(\widehat{\mathbb{O}}_{k,\theta}^{i,j} | \widehat{\mathbb{O}}_{i,j}) P(\widehat{\mathbb{O}}_{i,j} | \mathbb{O}_{x,y}) \\ &\quad \left. + P(S_{k,\theta} = 0 | \mathbb{O}_{k,\theta}^{i,j}) P(\mathbb{O}_{k,\theta}^{i,j} | \widehat{\mathbb{O}}_{i,j}) P(\widehat{\mathbb{O}}_{i,j} | \mathbb{O}_{x,y}) \right\} \quad (12) \end{aligned}$$

$$\begin{aligned} &= \left(1 - f + a_{k,\theta}^{x,y}(f - p_k)\right) \left\{ \prod_{i=1}^m \prod_{j=1}^n \left\{ \left(1 - f + a_{k,\theta}^{x,y}(f - p_k)\right) P(\mathbb{O}_{i,j}) \right. \right. \\ &\quad \left. \left. + (1 - f) P(\widehat{\mathbb{O}}_{i,j}) \right\} \right\} \forall (i, j) \neq (x, y) \quad (13) \end{aligned}$$

$$P(S_{k,\theta} = 1) = 1 - P(S_{k,\theta} = 0) \quad (14)$$

$$\begin{aligned} P(S_{k,\theta} = 0) &= \prod_{i=1}^m \prod_{j=1}^n \left\{ \sum_{\mathbb{O}_{i,j}} \sum_{\widehat{\mathbb{O}}_{k,\theta}^{i,j}} P(S_{k,\theta} = 0 | \mathbb{O}_{k,\theta}^{i,j}) P(\mathbb{O}_{k,\theta}^{i,j} | \mathbb{O}_{i,j}) P(\mathbb{O}_{i,j}) \right\} \\ P(S_{k,\theta} = 0) &= \prod_{i=1}^m \prod_{j=1}^n \left\{ \left(1 - f + a_{k,\theta}^{x,y}(f - p_k)\right) P(\mathbb{O}_{i,j}) \right. \\ &\quad \left. + (1 - f) P(\widehat{\mathbb{O}}_{i,j}) \right\} \quad (15) \end{aligned}$$

where $P(S_{k,\theta} = 1 | \mathbb{O}_{x,y})$ denotes the likelihood of getting a measurement $z_{k,\theta} \geq t_k$ from range bin (k, θ) given $O_{x,y}$ is already occupied and $P(S_{k,\theta} = 1)$ is the normalizing constant. $a_{k,\theta}^{i,j}$ becomes zero when the occupancy cell is far away from the range bin (k, θ) . Hence, we only update the probabilities within the neighborhood of $r \times r$ occupancy cells that enclose range bin (k, θ) . Also, while updating each occupancy cell $O_{x,y}$ in the $r \times r$ neighborhood, only the other occupancy cells $O_{i,j}$ in the same neighborhood will be involved.

It should be noted that for the case when $S_{k,\theta} = 1$, all possible combinations of detections and/or false alarms from all possible combinations of overlapping occupancy cells need to be considered. Hence calculating $P(S_{k,\theta} = 1)$ becomes rather involved. But $S_{k,\theta} = 0$ occurs only when a detection was missed or there was no target present in **all** the overlapping cells for which the probability can be calculated in a straightforward manner. Following which, $P(S_{k,\theta} = 1)$ can be calculated

by taking the compliment of $P(S_{k,\theta} = 0)$.

Case 2: When the measurement obtained is such that $S_{k,\theta} = 0$ ($z_{k,\theta} < t_k$), the occupancy cell $O_{x,y}$ is updated in a slightly different manner.

$$P(\mathbb{O}_{x,y}|S_{k,\theta} = 0) = \frac{P(S_{k,\theta} = 0|\mathbb{O}_{x,y})P(\mathbb{O}_{x,y})}{P(S_{k,\theta} = 0)} \quad (16)$$

where $P(S_{k,\theta} = 0|\mathbb{O}_{x,y})$ denotes the likelihood of getting a measurement $z_k < t_k$ from a range bin (k, θ) given $O_{x,y}$ is occupied. It can be obtained as per Eq. 12 and the normalizing constant, $P(S_{k,\theta} = 0)$, can be obtained from Eq. 15.

The implicit assumption made in the formulation is that the probabilities with which the cells are occupied are independent from one another.

2.3 Motion model

The motion model takes into account the translation and the rotational motion of the AUV and tracks the probabilities of the occupancy cells accordingly. It is defined such that the translational motion and rotational motion are decoupled from one another.

Translational Motion We model the translational motion as a convolution between the cell probabilities and an appropriate kernel \mathbf{K} . The choice of kernel K depends on whether the AUV undergoes deterministic or probabilistic motion.

Deterministic Motion: It is reasonable to model the AUV's motion as deterministic when GPS is available due to the high accuracy of GPS signals. For such a case, the occupancy grid is simply shifted by the amount of displacement. Fig. 3 shows how the probability is updated through a convolution when the robot undergoes translational motion.

The kernel is a representation of the amount of displacement the robot has undergone. In our case, the kernel is two dimensional represented by an $N \times N$ matrix. Elements of the kernel, which is the area of overlap, are shown in Fig. 3. The mathematical form of the motion update is as follows:

$$\mathbf{P} \otimes \mathbf{K} \quad (17)$$

where \otimes is the convolution symbol and \mathbf{P} is the matrix representation of the entire occupancy grid.

Probabilistic Motion: When there is no GPS or DVL available, the displacement is unimodal with its peak representing the mean translational motion, and spread modelling the uncertainty associated with the motion estimate. The uncertainty is modeled as a Gaussian distribution, denoted by $\mathcal{N}(\boldsymbol{\mu}, \mathbf{R})$ where $\boldsymbol{\mu}$ is the mean displacement of the AUV and variance, \mathbf{R} , is the process noise of the thruster model. Hence the area under the distribution would give the desired kernel \mathbf{K} . A typical element for this type of kernel would be of the form:

$$\mathbf{K}_{ij} = \iint_A \mathcal{N}(\boldsymbol{\mu}, \mathbf{R}) dx dy \quad (18)$$

The integral is evaluated over the region of the distribution represented by the element K_{ij} . The grid is updated using Eq. 17.

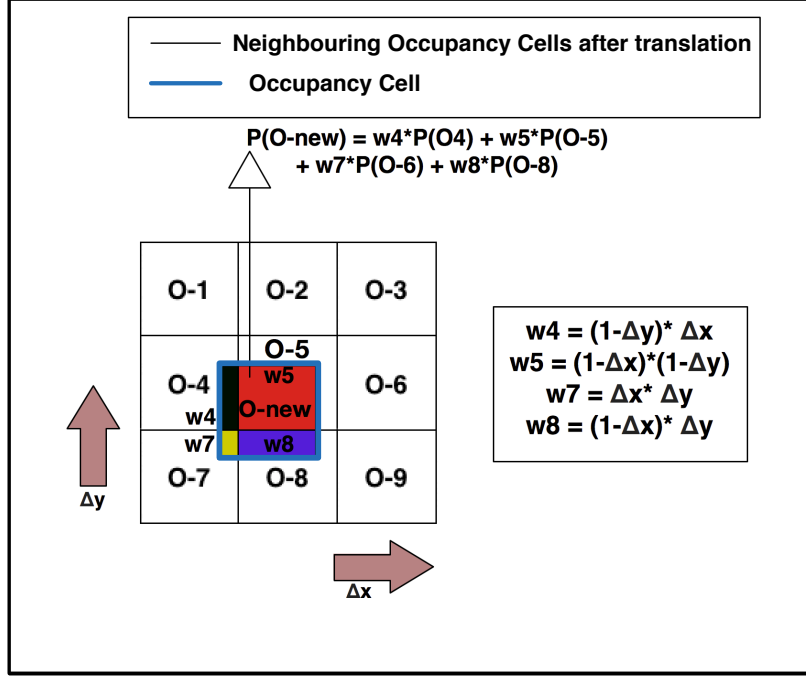


Fig. 3: Illustration of overlap of neighboring occupancy cells after undergoing translation with a particular occupancy cell. The area of overlap between O-new and O- $\{i\}$, is $w-\{i\}$ where $i \in \{4, 5, 7 \text{ and } 8\}$.

Rotational Motion We model the rotational motion of the AUV as deterministic. To avoid rounding errors, we accumulate changes in heading until they reach $\pm 1^\circ$. The area of overlap of rotated neighboring occupancy cells $O'_{x-i,y-j} \forall i, j \in \{-1, 0, 1\}$ with a particular occupancy cell $O_{x,y}$ is calculated. Then the new probability of occupancy is updated as:

$$P(\mathbb{O}_{x,y}) = \sum_i \sum_j w_{x,y}^{x-i,y-j} P(\mathbb{O}'_{x-i,y-j}) \quad (19)$$

where $w_{x,y}^{x-i,y-j}$ is the ratio of the area of overlap between occupancy cell $O'_{x-i,y-j}$ and $O_{x,y}$ and the area of occupancy cell $O_{x,y}$. Fig. 4 shows how the probability is updated in the presence of rotation.

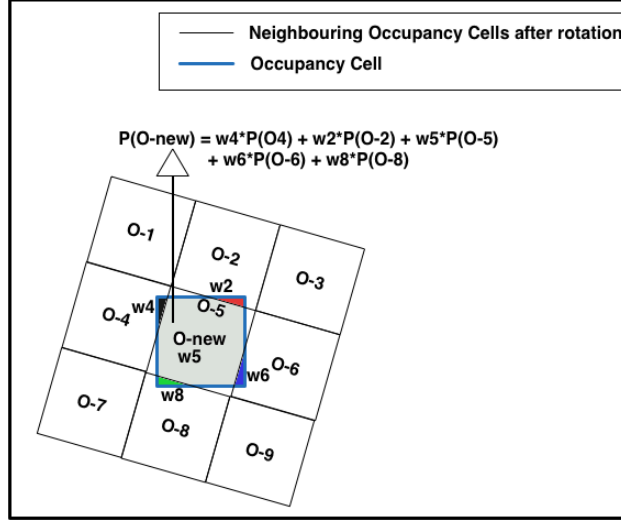


Fig. 4: Illustration of overlap of neighboring occupancy cells after undergoing rotation with a particular occupancy cell. The area of overlap between O-new and O- $\{i\}$, is $w-\{i\}$ where $i \in \{2, 4, 5, 6 \text{ and } 8\}$.

2.4 Obstacle Detection

The expected number of obstacles $N_{x,y}$ in a neighborhood of a occupancy cell $O_{x,y}$ can be estimated from the occupancy grid:

$$N_{x,y} = \sum_i \sum_j P(O_{x-i,y-j}) \forall i, j \in \{-1, 0, 1\}. \quad (20)$$

Here we have taken the neighborhood to be ± 1 . We set a threshold P_{thresh} and declare a detected obstacle if $N_{x,y} \geq P_{\text{thresh}}$. At the end of every scan, the obstacles detected throughout the grid is sent to the Navigator of the AUV to carry out necessary avoidance maneuvers if necessary.

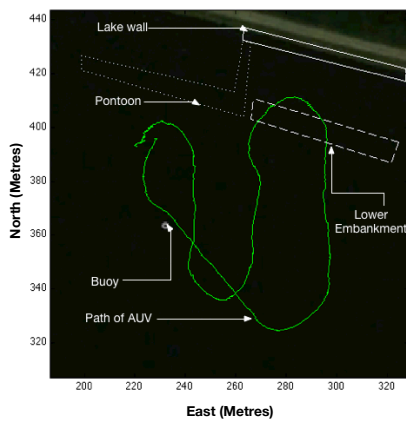
3 Experimental Setup

We conducted experiments at Pandan reservoir in Singapore and also in the sea off the coast of Singapore. For both sets of experiments, we used a Micron DST sector scanning sonar [16] integrated on our STARFISH AUV [17].

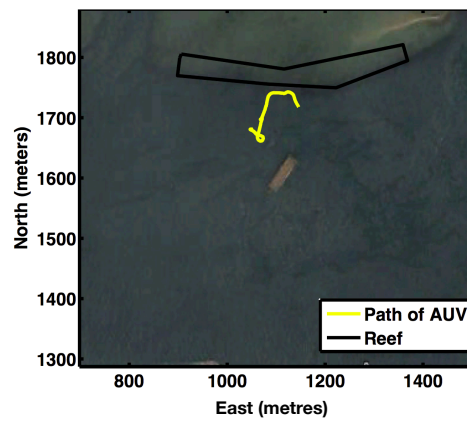
During the Pandan experiment, the mission was planned such that the AUV would be operating near some static buoys and the reservoir's embankments. The sonar was configured for 50 m operating range with 44 bins and 90° scan sector. The mission was executed with the AUV maintaining a constant depth of 0.5 m. The mission path and the

obstacles in the environment are shown in Fig. 5(a). Note that the lower embankment wall is not visible from the surface but marked in Fig. 5(a) using a dashed line. A illustration of the cross-section of the embankment is shown in Fig. 5(c).

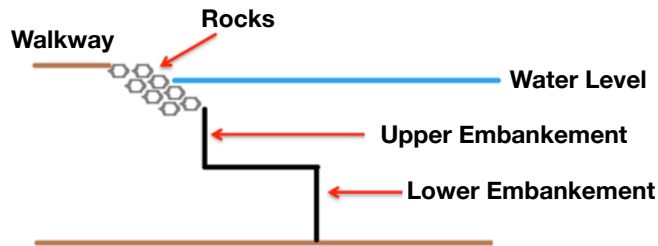
The experiment at sea was conducted at Selat Pauh, an anchorage area south of Singapore with a depth of 10-20 m. The AUV mission plan led the AUV to an area close to shallow coral reefs (< 5 m). During this mission, the AUV swam at the surface. Fig. 5(b) shows the AUV path and the location of the shallow reefs.



(a) AUV path and obstacle locations at Pandan reservoir



(b) AUV path and reef location at sea



(c) Illustration showing the structure of embankments at Pandan reservoir

Fig. 5: Experiments at Pandan reservoir and at sea

4 Results

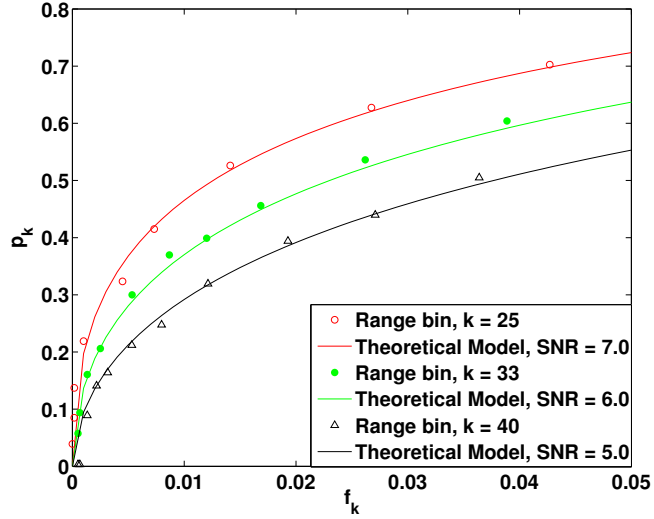
The experimentally obtained ROC curves at Pandan reservoir matched those obtained from a Gaussian noise model with an appropriate SNR at operational values of f_k (0.01-0.04) as shown in Fig. 6(a). We set the desired false alarm rate $f = 0.02$ and obtained p_k and t_k values for all range bins. The scans from the FLS were processed online and local occupancy grids were generated. Obstacles such as the reservoir embankments and buoys were clearly detected. Unprocessed scans, local occupancy grids and obstacle detections are shown in Fig. 7 (first, second and third row).

The ROC curves obtained from the experiments held at the sea are shown in Fig. 6(b) for operational values of f_k . As the sea was much noisier than the reservoir, we set a slightly higher rate of false alarm $f = 0.03$ to ensure good detections. The FLS scans were processed in the same way as the Pandan experiment, and the results are shown in Fig. 7 (bottom row).

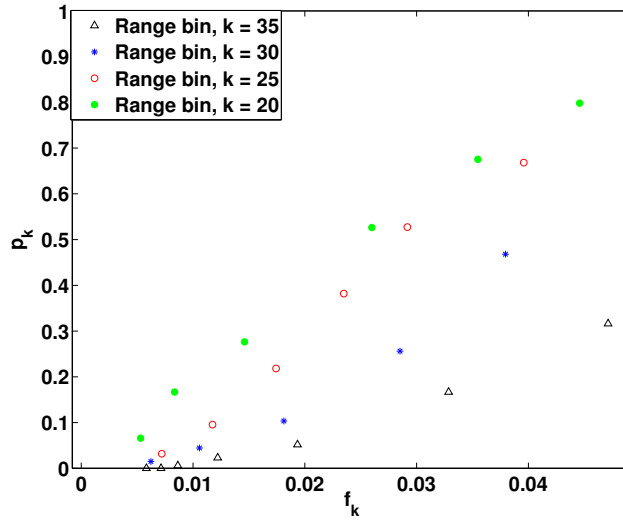
5 Experimental Insights

From the unprocessed sonar scans shown in Fig. 7 (left column), we see that the targets cannot be clearly distinguished from the background noise. Multiple scans are processed and assimilated into the local occupancy grid as the AUV moves. The results from this process are seen in Fig. 7 (middle column). We observe that the cells corresponding to obstacles show a high probability of occupancy. The improvement comes from combining information from multiple scans. The Bayesian update effectively weighs the information from multiple scans based on its reliability. Finally, a hard-decision detection procedure is used at the end of each scan to detect potential obstacles. Obstacles such as buoys, reservoir embankments and coral reefs are detected reliably as shown in Fig. 7 (right column). These obstacle detections are then sent to the AUV's command and control system.

While Bayesian updates of an occupancy grid can be implemented in a geo-referenced frame, accumulation of errors in the AUV's position estimate can render this approach ineffective. By noting that obstacle avoidance only requires accurate knowledge of obstacle locations in an AUV's body frame, we are able to use a local occupancy grid in concert with a uncertainty-aware motion model. The result is an algorithm that accurately tracks and detects obstacles in the AUV's frame of reference. Although this approach is ideally suited to obstacle avoidance, it does not provide an absolute location for each detected obstacle and therefore is unsuitable for mapping applications. The approach limits the occupancy grid to a small region around the AUV; this limits memory requirements and computational load and makes the algorithm appropriate for real-time implementation. However it also results in the AUV "forgetting" obstacles that it might have seen during a previous visit to a given area. Since revisiting areas is not common during most AUV missions, and



(a) ROC plot at Pandan Reservoir and the corresponding theoretical curves



(b) ROC plot at Selat Pauh

Fig. 6: Experimentally obtained ROC plots.

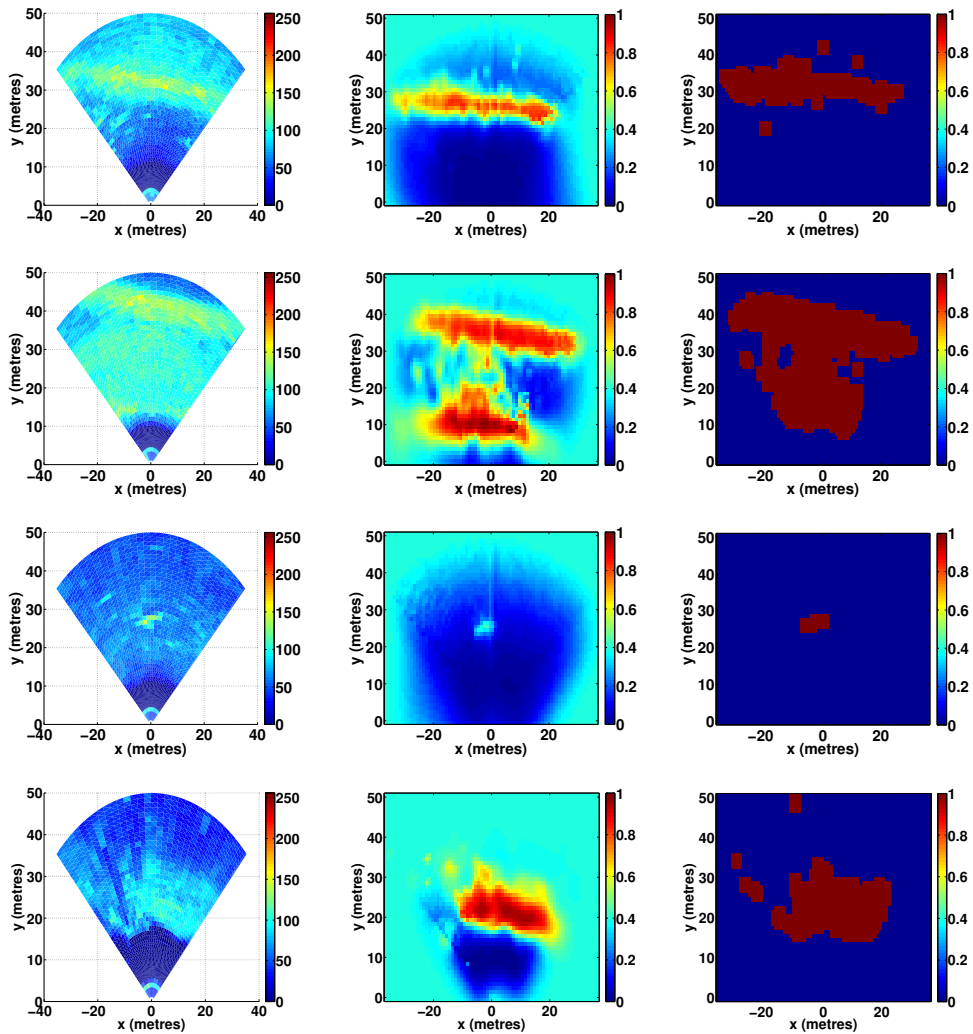


Fig. 7: Unprocessed scans (left column), occupancy grid (middle column) and obstacle detection (right column) of various targets. The first two rows show the reservoir’s embankments during the Pandan experiment, while the third row shows a buoy during the same experiment. The bottom row shows a patch of coral reef during the sea experiment.

since obstacles can be reliably re-detected, we do not see this as a significant shortcoming. We therefore believe that our proposed algorithm is well suited to underwater obstacle detection and collision avoidance for AUVs, and can be not only used with expensive multibeam sonars, but also with cheaper sector scanning FLS.

6 Conclusion

We developed a novel method for underwater obstacle detection using a probabilistic local occupancy grid. We demonstrated its capability to detect obstacles robustly and localize them accurately in the AUV's frame of reference. Compared to previous published approaches, our approach deals more directly with positional uncertainty by adopting an occupancy grid in the AUV's frame of reference. Hence, the obstacles are accurately localized relative to the AUV. Finally, this method is computationally less intensive compared to other image processing techniques or SLAM techniques and can be implemented on board an AUV. Future work may explore the possibility of tackling the problem of the "forgetting" nature of the local occupancy grid.

References

1. T. Y. Teck and M. Chitre, "Direct Policy Search With Variable-Length Genetic Algorithm for Single Beacon Cooperative Path Planning," in *International Symposium on Distributed Autonomous Robotic Systems (DARS)*, November 2012.
2. S. Thrun, W. Burgard, and D. Fox, *Probabilistic Robotics (Intelligent Robotics and Autonomous Agents)*. The MIT Press, 2005.
3. J. C. Leedekerken, J. J. Leonard, M. C. Bosse, and A. Balasuriya, "Real-time obstacle avoidance and mapping for AUVs operating in complex environments," in *Proceedings of the 7th International Mine Warfare Symposium, Monterey, CA*, 2006.
4. E. Brekke and M. Chitre, "Bayesian Multi-Hypothesis Scan Matching," in *Proceedings of OCEANS'13*, Bergen, Norway, June 2013.
5. A. Elfes, "Using occupancy grids for mobile robot perception and navigation," *Computer*, vol. 22, no. 6, pp. 46–57, June 1989.
6. K. Konolige, "Improved occupancy grids for map building," *Autonomous Robots*, vol. 4, no. 4, pp. 351 – 67, 1997.
7. A. Eliazar, "DP-SLAM," Ph.D. dissertation, Department of Computer Science, Duke University, 2005.
8. D. P. Horner, A. J. Healey, and S. P. Kragelund, "AUV experiments in Obstacle Avoidance," in *Proceedings of MTS/IEEE OCEANS*, September 2005.
9. I. Quidu, A. Hetet, Y. Dupas, and S. Lefevre, "AUV (Redermor) obstacle detection and avoidance experimental evaluation," in *OCEANS 2007 - Europe*, Aberdeen, UK, 2007.
10. K. Teo, K. W. Ong, and H. C. Lai, "Obstacle detection, avoidance and anti collision for MEREDITH AUV," in *MTS/IEEE Biloxi - Marine Technology for Our Future: Global and Local Challenges, OCEANS 2009*, Biloxi, MS, USA, 2009.

11. H. Heidarsson and G. Sukhatme, "Obstacle detection and avoidance for an Autonomous Surface Vehicle using a profiling sonar," in *IEEE International Conference on Robotics and Automation (ICRA)*, 2011.
12. A. Martin, E. An, K. Nelson, and S. Smith, "Obstacle detection by a forward looking sonar integrated in an autonomous underwater vehicle," in *Oceans 2000*, vol. 1, Providence, RI, USA, 2000.
13. J. L. Chew and M. Chitre, "Object Detection with Sector Scanning Sonar," in *Proceedings of OCEANS'13*, San Diego, CA, USA, September 2013.
14. "Robocentric map joining: Improving the consistency of EKF-SLAM," *Robotics and Autonomous Systems*, vol. 55, no. 1, pp. 21–29, January 2007.
15. M. Richards, "Fundamentals of radar signal processing," pp. 304–316, 2005.
16. Tritech. Micron DST sector scanning sonar. [Online]. Available: <http://www.tritech.co.uk/product/small-rov-mechanical-sector-scanning-sonar-tritech-micron>
17. T. Koay, Y. Tan, Y. Eng, R. Gao, M. Chitre, J. Chew, N. Chandhavarkar, R. Khan, T. Taher, and J. Koh, "STARFISH—A Small Team of Autonomous Robotic Fish," *Indian Journal of Geo-Marine Sciences*, vol. 40, no. 2, pp. 157–167, 2011.